BIOCHEMISTRY
including biophysical chemistry & molecular biology

Article

pubs.acs.org/biochemistry

Substrate-Mediated Oxygen Activation by Homoprotocatechuate 2,3-Dioxygenase: Intermediates Formed by a Tyrosine 257 Variant

Michael M. Mbughuni,[†] Katlyn K. Meier,[§] Eckard Münck,*[,§] and John D. Lipscomb*[,†]

[†]Department of Biochemistry, Molecular Biology and Biophysics and Center for Metals in Biocatalysis, University of Minnesota, Minneapolis, Minnesota 55455, United States

[§]Department of Chemistry, Carnegie Mellon University, Pittsburgh, Pennsylvania 15213, United States

Supporting Information

ABSTRACT: Homoprotocatechuate (HPCA; 3,4-dihydroxyphenylacetate or 4-carboxymethyl catechol) and O_2 bind in adjacent ligand sites of the active site Fe^{II} of homoprotocatechuate 2,3-dioxygenase (FeHPCD). We have proposed that electron transfer from the chelated aromatic substrate through the Fe^{II} to O_2 gives both substrates radical character. This would promote reaction between the substrates to form an alkylperoxo intermediate as the first step in aromatic ring cleavage. Several active site amino acids are thought to promote these reactions through acid/base chemistry, hydrogen bonding, and electrostatic interactions. Here the role of Tyr257 is explored by using the Tyr257Phe (Y257F) variant, which decreases k_{cat} by about 75%. The crystal structure of the FeHPCD-HPCA complex has shown that Tyr257 hydrogen bonds to the deprotonated C2-hydroxyl of HPCA. Stopped-flow studies show that at least two reaction intermediates, termed $Y257F_{Int1}^{HPCA}$ and $Y257F_{Int2}^{HPCA}$, accumulate during the Y257F-HPCA + O_2 reaction prior to formation of the ring-cleaved product. $Y257F_{Int1}^{HPCA}$ is colorless and is formed as O_2 binds reversibly to the HPCA−enzyme complex. $Y257F_{Int2}^{HPCA}$ forms spontaneously from $Y257F_{Int1}^{HPCA}$ and displays a chromophore at 425 nm (ε_{425} = 10 500 M^{-1} cm^{-1}). Mössbauer spectra of the intermediates trapped by rapid freeze quench show that both intermediates contain Fe^{II}. The lack of a chromophore characteristic of a quinone or semiquinone form of HPCA, the presence of Fe^{II}, and the low O_2 affinity suggest that $Y257F_{Int1}^{HPCA}$ is an HPCA-Fe^{II}-O_2 complex with little electron delocalization onto the O_2. In contrast, the intense spectrum of $Y257F_{Int2}^{HPCA}$ suggests the intermediate is most likely an HPCA quinone-Fe^{II}-(hydro)peroxo species. Steady-state and transient kinetic analyses show that steps of the catalytic cycle are slowed by as much as 100-fold by the mutation. These effects can be rationalized by a failure of Y257F to facilitate the observed distortion of the bound HPCA that is proposed to promote transfer of one electron to O_2.

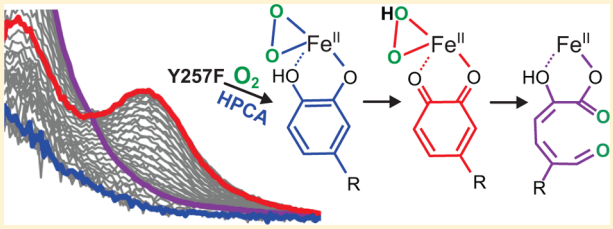

Homoprotocatechuate 2,3-dioxygenase (FeHPCD) from *Brevibacterium fuscum* catalyzes the insertion of both atoms from O_2 into the aromatic ring of homoprotocatechuate (HPCA, 3,4-dihydroxyphenylacetate or 4-carboxymethyl catechol) resulting in ring-opening as shown in Scheme 1.[1,2]

The enzyme utilizes an Fe^{II}, which is bound in the active site by two histidine and one glutamic acid side chains in a 2-His-1-carboxylate facial triad motif shown in Figure 1A.[3−7] Substrates bind in multistep processes to displace solvents from the Fe^{II} and form a chelate complex.[8] For catecholic substrates such as HPCA with relative high pK_a values for the hydroxyl substituents, only the C2-hydroxyl group deprotonates upon binding, so that the overall charge of the metal center is neutral.[3−5,9] Crystallographic studies have shown that small molecules such as O_2 and the O_2 surrogate NO bind in the open ligand site of the Fe^{II} adjacent to the substrate.[5,6] We and others have proposed the mechanism summarized in Scheme 1 in which an electron is transferred from the aromatic substrate through the iron to the oxygen, giving both substrates radical character ($SQ^{\bullet}$-Fe^{II}-$O_2^{\bullet-}$).[8,10−14] Recombination of the radicals would yield an alkylperoxo intermediate. A subsequent Criegee-type rearrangement would result in O−O bond cleavage to yield a substrate lactone intermediate with the second atom of

Scheme 1. Proposed Reaction Sequence for Extradiol Dioxygenases[a]

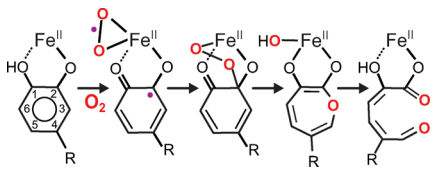

[a]For the studies described here, R = CH_2COO^-. The numbering system shown is adopted for consistency with studies described in the accompanying report.[2] The endogenous Fe^{II} ligands are omitted for clarity.

Received: August 16, 2012
Revised: October 12, 2012
Published: October 15, 2012

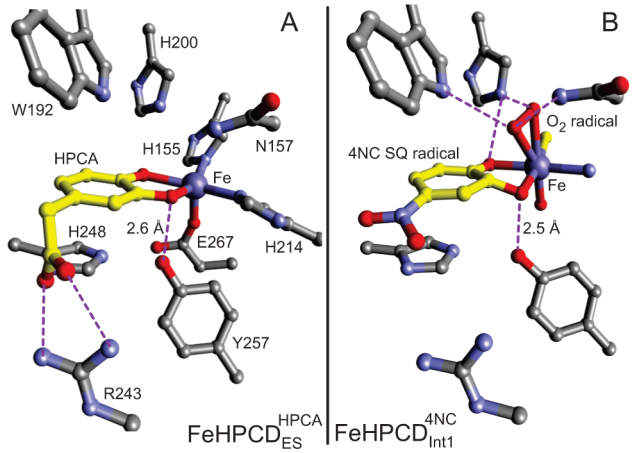

Figure 1. Second sphere residues proposed to participate in catalysis. (A) $FeHPCD^{HPCA}_{ES}$, structure of the anaerobic FeHPCD-HPCA substrate complex (PDBID: 1Q0C).[3] (B) $FeHPCD^{4NC}_{Int1}$, structure of the oxy complex from the FeHPCD-4NC + O_2 reaction (PDBID: 2IGA, subunit C).[6] This reaction intermediate is proposed to have a $SQ^{\bullet}$-Fe^{II}-$O_2^{\bullet-}$ electronic structure. The endogenous iron ligands are omitted for clarity.

oxygen retained on the iron. Hydrolysis of the lactone by this oxygen would yield the bound product ready for release.

Crystallographic studies in which the slow alternative substrate 4-nitrocatechol (4NC) was diffused anaerobically into the crystal and the reaction initiated by exposure to low concentrations of O_2 have allowed the $SQ^{\bullet}$-Fe^{II}-$O_2^{\bullet-}$ (Figure 1B), alkylperoxo, and the product complexes to be structurally characterized.[6] A gem-diol intermediate (or stabilized form), which presumably occurs between the alkylperoxo and lactone intermediates, was trapped in a crystal and structurally characterized using a similar approach.[15] These studies and earlier structural studies of the FeHPCD−HPCA complex[3] have revealed several residues in the active site that are likely to facilitate catalysis (Figure 1A). In particular, residue His200 is positioned to interact with both the substrate C1-OH substituent and the bound oxygen. Mutation of this residue indicates that it plays many roles including that of an acid−base catalyst to promote the Criegee rearrangement chemistry.[12] It may also serve to sterically promote the side-on binding orientation of the oxygen in the $SQ^{\bullet}$-Fe^{II}-$O_2^{\bullet-}$ complex revealed by the crystal structure and to stabilize the oxy complex by a combination of hydrogen bonding and charge interaction with the bound superoxo anion (Figure 1B). Substitution of His200 by shorter residues that cannot effectively hydrogen bond or catalyze acid−base chemistry and/or the use of alternative substrates greatly slow catalysis, allowing several intermediates to be trapped by rapid freeze quench (RFQ) techniques for spectroscopic characterization.[16,17]

Another active site residue, Tyr257, also appears to be important for catalysis based on its interaction with the HPCA C2−O^-. This residue is located on the opposite side of the substrate from His200 and forms a hydrogen bond with the deprotonated substrate hydroxyl (Figure 1A). We postulate that Tyr257 promotes oxygen activation, ring attack, and ring cleaving chemistry in several ways related to favoring a tetrahedral geometry at the carbon bearing this hydroxyl. This proposal is based on the observation that the structurally characterized intermediates exhibit an increasingly tetrahedral substrate C2 as they progress toward product formation (see for example Figure 1B).[6,15] Consequently, active site structural elements that favor sp^3 hybridization at substrate C2 should promote each step of the reaction.

Here we explore the roles of Tyr257 in catalysis by mutating it to a Phe (Y257F), which preserves the spatial characteristics of Tyr, but not the ability to hydrogen bond or sterically interact with the substrate via the Tyr hydroxyl substituent. It is found that, in accord with the postulated role for Tyr257, the Y257F-HPCA + O_2 reaction forms a ring-cleaved product with kinetics that are slow in comparison to those of the wild-type reaction. The slow internal steps of the Y257F reaction cycle allow new intermediates to be detected, trapped, and characterized. The new intermediates support the proposed requirement for electron transfer to the oxygen from the substrate without a net change in metal oxidation state prior to O_2 attack in order to sustain efficient catalysis. The structural basis for the roles of Tyr257 are explored in the accompanying report.[2]

EXPERIMENTAL PROCEDURES

Reagents and Enzymes. All chemicals were purchased from Sigma-Aldrich and were used without purification except for HPCA which was recrystallized from water at 4 °C to remove minor contaminants. Anaerobic conditions were achieved by repeated cycling of solutions between argon gas and vacuum. Trace contaminating O_2 was removed from the Ar gas by passage through an Agilent GC-1 POP O_2 scrubbing cartridge, then through an Agilent GC-4 POP O_2 indicating cartridge. Mushroom tyrosinase was purchased from Sigma-Aldrich.

Y257F Variant. Y257F mutant of FeHPCD was prepared using the Stratagene QuickChange kit. The following mutagenesis primer was used along with its reverse complement:

GCGTCTCCAACGCGTTCTACCTG**TTC**ATCC

The mutant codon is shown in bold highlight. The mutation was confirmed via sequencing at the University of Minnesota MicroChemical Facility.

Recombinant WT FeHPCD and Y257F were purified as previously described[1,12] with a few modifications. No cysteine or Fe was added to the purification buffers, but all buffers used in the purification were continually sparged with 1 psi of N_2 to remove O_2. After loading FeHPCD onto the DEAE Sepharose column, the column was gravity washed with 10 column volumes of buffer (50 mM MOPS pH 6.8 + 190 mM NaCl). The wash buffer is sparged with 1 psi of N_2 during this process. After the wash, a salt gradient totaling 10 column volumes was run from 190−350 mM NaCl using a gravity dependent gradient maker sparged with 1 psi N_2 in the mixing chamber (chamber with low salt buffer). The pooled fractions from the DEAE Sepharose column were found to be sufficiently pure for kinetic and spectroscopic studies. Purified Y257F yielded the correct ring cleaved product from HPCA.

The isotope ^{57}Fe was incorporated into the enzyme by growth on ^{57}Fe enriched media as previously described except that the media contained 4 g/L yeast extract and 4 mL/L of filter sterilized glycerol.[16] Mössbauer analysis of the purified Y257F mutant revealed ∼1 eq of $^{57}Fe^{II}$/site enrichment as previously described for the wild type enzyme and the H200N mutant.[16,17]

Iron Quantification Using ICP-OES. The ICP-OES samples are digested in 20% nitric acid at 37 °C for at least 24 h. Insoluble materials were removed by centrifugation at

dx.doi.org/10.1021/bi301114x | Biochemistry 2012, 51, 8743−8754

Table 1. Steady-State Parameters for FeHPCD-HPCA and Y257F-HPCA Reaction with O_2[a]

kinetic parameter	wild type 22 °C pH 7.5	Y257F 22 °C pH 7.5	Y257F 4 °C pH 7.5	Y257F 22 °C pH 5.5
k_{cat} (s^{-1})	10.0 ± 1.5	2.70 ± 0.13	0.38 ± 0.07	0.4 ± 0.1
K_m^{HPCA} (mM)	0.016[b]	0.26 ± 0.05	0.25 ± 0.05	0.13 ± 0.02
k_{cat}/K_m^{HPCA} (mM^{-1} s^{-1})	625	10.4	1.5	3.1
$K_m^{O_2}$ (mM)	0.015 ± 0.007	0.08 ± 0.03	0.02 ± 0.01	0.01 ± 0.005
$k_{cat}/K_m^{O_2}$ (mM^{-1} s^{-1})	667	34	19	40

[a]Reactions were conducted in 200 mM MES or MOPS at pH 5.5 or 7.5, respectively. The buffer is air saturated at either 4 or 22 °C. At this O_2 concentration, the reaction is saturated. [b]From ref 1.

10000*g* at 4 °C. The supernatant was analyzed for transition metals using ICP-OES at the Aqueous Geochemistry Lab (University of Minnesota, Department of Earth Science).

Stopped-Flow Kinetics and Spectroscopy. All stopped-flow experiments were performed using an Applied Photophysics model SX.18MV stopped-flow device. The reaction procedures were as previously described.[8] All stopped-flow experiments were conducted at 4 °C in 50 mM MOPS buffer at pH 7.5 or 50 mM MES buffer at pH 5.5, as previously described.[17] Solutions varying in O_2 concentrations were prepared by diluting a stock saturated O_2 buffer solution with anaerobic buffer in a gastight 5 mL Hamilton syringe equilibrated on ice. The kinetic data were analyzed to extract reciprocal relaxation times using the Applied Photophysics Pro-Data Viewer version 4.0.17. In general, the reaction time courses were fit to summed exponential expressions, which are appropriate for series of first order or pseudo first order reactions.[18] EPR spectra were collected using a Bruker Elexsys E-500 spectrometer equipped with a Bruker dual mode cavity and an Oxford ESR 910 liquid helium cryostat. Mössbauer spectroscopy was performed as previously described.[16,19] Spectra were analyzed using the software WMOSS (SEE Co, Edina, MN, USA).

Steady-State Kinetic Experiments. Steady-state kinetic parameters for the ring-cleaving reaction of FeHPCD and the Y257F variant were monitored using UV−vis detection. The initial velocity of product formation was observed at 380 nm using a stopped-flow device. The linear portion of the trace was fit using the Pro Data Viewer software package. The enzyme concentration was 1 μM for FeHPCD and 3−6 μM for Y257F after mixing with varying HPCA substrate concentrations. Experiments were done at either 4 or 22 °C in 200 mM MES or MOPS buffer at pH 5.5 or pH 7.5, respectively, in air saturated buffer as noted in the figure legends. Initial velocities were fit as a hyperbolic function of substrate concentration to determine K_m and V_{max} using the data analysis software in Origin.

Rapid Freeze Quench (RFQ) Methods. Y257F-HPCA anaerobic complex (1.6 mM) was prepared in the glovebox by mixing 1 equiv of Y257F with 1 equiv of HPCA. RFQ syringes were loaded inside the Coy anaerobic glovebox and then transferred to an Update Instrument model 1019 RFQ apparatus and allowed to equilibrate for 30 min at 4 °C. The RFQ samples were mixed with O_2 buffer as previously described.[17] Previously, we observed a splash artifact when the shortest time reaction mixtures were frozen on the counter-rotating aluminum wheels maintained at liquid N_2 temperature.[17] To avoid this artifact, the instrument was redesigned to rotate the wheels at a higher velocity and plastic scrapers were placed to remove the frozen solution from the wheels each cycle. This allowed the reaction mixture to always contact the metal surface rather than frozen solution on the wheel. Samples at times >1 s were frozen as previously described.[17]

Preparation of HPCA Semiquinone and HPCA Quinone. HPCA was oxidized to a quinone using mushroom tyrosinase (Sigma) in 100 mM MOPS buffer pH 7.5 and 4 °C. A solution of 2 mM HPCA was mixed with 10 mg/mL mushroom tyrosinase. The quinone formed during the first 4 min of the reaction. It is photolabile and decays to an unidentified secondary species over the next 10 min. HPCA was oxidized to a transient semiquinone by oxidation with 3,4,5,6-tetrachloro-1,2-benzoquinone (O-chloranil, Sigma-Aldrich) in ethanol at 20 °C.[20,21] The reaction was initiated and monitored using the stopped-flow spectrometer with diode-array detection (2 mm path). A solution of 2 mM HPCA was mixed with 2 mM of O-chloranil. The semiquinone formed during the first 150 s of the reaction and then slowly decayed to an unidentified species.

RESULTS

The Y257F Variant of FeHPCD Reacts Slowly. The steady-state parameters for Y257F with the HPCA substrate were determined at 4 and 22 °C and at pH 7.5 and pH 5.5 by monitoring the initial velocity of product formation using stopped-flow spectroscopy as summarized in Table 1. An example of the Michaelis−Menten plot for HPCA varied at pH 7.5 and 4 °C is shown in Figure S1. The results show that the k_{cat} value decreases to about 27% of that of the WT enzyme at pH 7.5, 22 °C. The K_m^{HPCA} is increased by about 16-fold by the mutation, whereas $K_m^{O_2}$ is increased only slightly.

Substrate Binds Tightly to Y257F. Direct determination of the K_d for HPCA is complicated by the lack of a visible or fluorescence change upon binding. However, the K_d can be approximated by comparison to 4NC binding. The K_d for 4NC for WT enzyme has been previously determined to be 5 μM based on the spectroscopic change that occurs as monoanionic 4NC in solution converts to the dianionic form bound to the enzyme.[8] The fraction of 4NC bound upon addition of a fixed concentration to Y257F is the same as that observed for the WT enzyme, showing that the K_d does not change significantly (Figure 2, blue and black traces). When HPCA and 4NC are added in equal concentrations to either FeHPCD or Y257F, only the spectrum of free 4NC is observed, showing that HPCA binds much more tightly than 4NC (K_d < 5 μM) in each case (Figure 2, red trace). This is not the case when a weak binding substrate 4-chlorocatechol (4CC) is added instead of HPCA (Figure 2, green and black traces). These results suggest that the relatively high K_m^{HPCA} value observed for Y257F must be attributed to reaction cycle steps other than those associated with formation of the final substrate complex. The low K_d value facilitates transient kinetic experiments as described below.

Single-Turnover Studies of the Y257F-HPCA + O_2 Reaction Reveal Two Reaction Intermediates. The diode-array stopped-flow spectra from an experiment wherein anaerobic, stoichiometric Y257F-HPCA complex reacts with a

dx.doi.org/10.1021/bi301114x | *Biochemistry* 2012, 51, 8743−8754

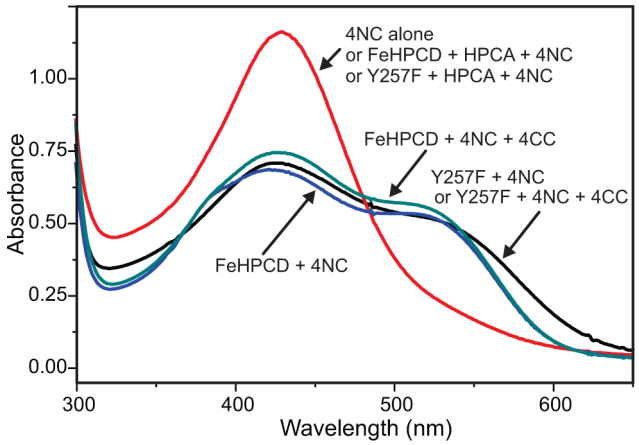

Figure 2. Estimation of K_d for HPCA binding to Y257F. The anaerobic substrate complexes were prepared in 200 mM MOPS buffer pH 7.5, 22 °C. 4CC is a weak binding catechol, 4-chlorocatechol. Concentrations: Y257F and FeHPCA, 40 μM; HPCA, 4NC, and 4CC, 80 μM when present.

large excess O_2 at 4 °C at pH 7.5 or pH 5.5 are shown in Figure 3, panels A and B, respectively. There is little change in the spectra in the first 30 ms at either pH value. Indeed, single wavelength data at 450 nm from pH 7.5 and pH 5.5 diode-array time courses clearly reveal a lag-phase during this period

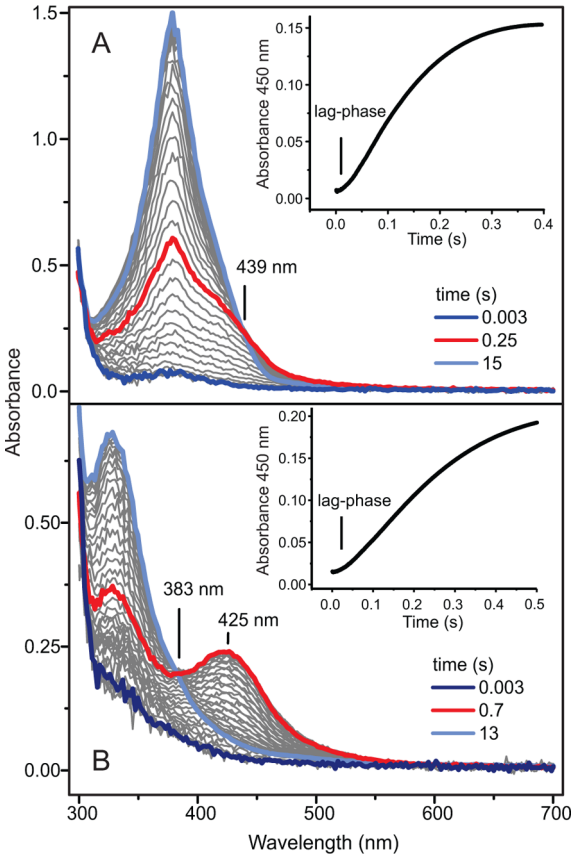

Figure 3. The Y257F-HPCA + O_2 reaction time-course followed using diode-array detection. Approximately 80 μM Y257F-HPCA complex was mixed with ~500 μM O_2 at 4 °C and pH 7.5 (A) and pH 5.5 (B) (1 cm path length). Inset: The reaction time-course monitored with single-wavelength detection at 450 nm.

(Figure 3A,B insets). This suggests that there is at least one colorless intermediate formed at the outset of the reaction before formation of a chromophoric species.

At slightly longer times, a transient species with a chromophore in the 400−470 nm range is observed. At pH 7.5, the chromophore begins to appear after 30 ms and maximizes at ~250 ms before it decays over the course of several seconds to yield the extradiol ring-cleaved product (λ_{max} = 380 nm). The spectrum of the transient species has an isosbestic point with that of the ring-cleaved product, so it may be the direct precursor of product formation in the reaction cycle. However, it is possible that other short-lived intermediates may intervene.

It was previously shown that λ_{max} for the ring-cleaved product shifts to a shorter wavelength at low pH.[17] Accordingly, when the Y257F-HPCA + O_2 reaction is conducted at pH 5.5, λ_{max} for the ring-cleaved product shifts to 325 nm, revealing the chromophore associated with the new intermediate at 425 nm (Figure 3B). The pH 5.5 data shows that the new intermediate maximizes at ~700 ms, suggesting one or both rate constants for formation and decay of this species have changed at low pH. We will term the first and second new intermediates $Y257F^{HPCA}_{Int1}$ and $Y257F^{HPCA}_{Int2}$, respectively.

Rate Constants for the Formation and Decay of the Intermediates. Single-wavelength kinetic time courses were analyzed using regression methods to obtain reciprocal relaxation times ($1/\tau$ values) associated with the reaction. Figure 4 shows the single wavelength time course monitored under pseudo first order conditions at 450 or 350 nm for the first 15 s of the Y257F-HPCA + O_2 reaction at pH 7.5 or 5.5, 4 °C. Each of the time courses requires four summed exponential phases to achieve a satisfactory fit (summarized in Table 2). The slowest phase is not kinetically competent and arises from a photochemical side reaction of the product bound to the enzyme as described in Supporting Information (Figure S2).

Observation of at least three competent phases in product formation at pH 5.5 and pH 7.5 shows that the Y257F-HPCA + O_2 single turnover reaction entails at least three distinct steps under both low and high pH conditions (Table 2). For a given pH, pairs of reciprocal relaxation times are similar at the two wavelengths monitored in all cases, suggesting that three phases are sufficient to describe the product formation time courses. The slower reciprocal relaxation times decrease with decreasing pH, albeit not proportionally, consistent with the slower formation and longer lifetime observed for the chromophoric intermediate $Y257F^{HPCA}_{Int2}$ at pH 5.5 (Figure 3A,B).

The reciprocal relaxation times for the reaction monitored at 425 nm are plotted vs the O_2 concentration in Figure 5. For the reaction at pH 5.5, it is seen that only $1/\tau_1$ is dependent on O_2 concentration and that the dependence is linear passing through zero (Figure 5A). The linear dependence suggests that $1/\tau_1$ is at least dominated by the rate constant for the O_2 binding step and the zero intercept suggests that this step is effectively irreversible. If the binding reaction occurs first in the reaction sequence and is irreversible, then $1/\tau_1 = k_1 = 4.0 \times 10^4 \pm 0.2\ M^{-1}\ s^{-1}$.

At pH 7.5, the fastest reciprocal relaxation time is again linearly dependent on O_2 concentration, but the intercept of the plot is not zero (Figure 5D). This is the expected result if the O_2 binding reaction occurs first and is reversible at this pH value. The forward and reverse rate constants are given by the slope and intercept of the plot respectively ($k_1 = 2.7 \times 10^4 \pm 0.2\ M^{-1}\ s^{-1}$, $k_{-1} = 11.0 \pm 0.1\ s^{-1}$, $K_d^{O_2} = k_{-1}/k_1 \approx 400\ \mu M$).

dx.doi.org/10.1021/bi301114x | Biochemistry 2012, 51, 8743−8754

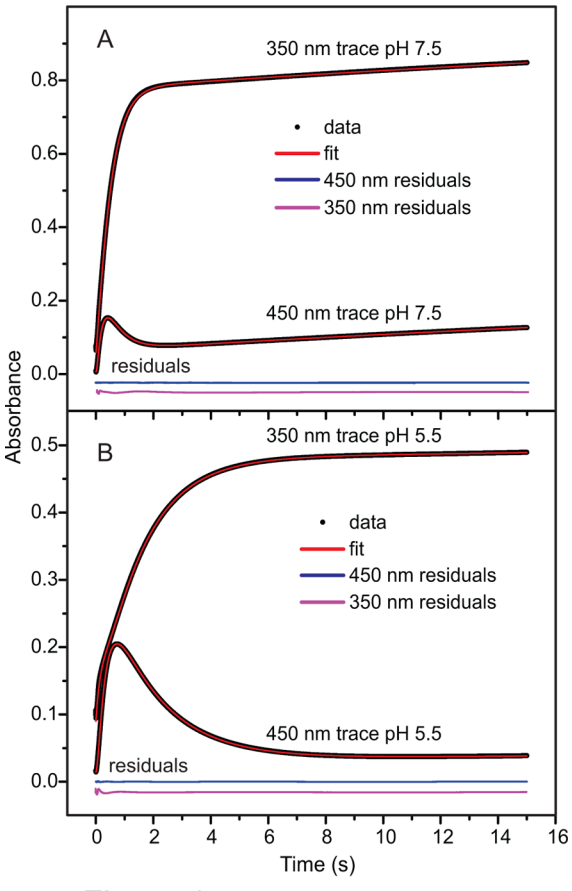

Figure 4. The Y257F-HPCA + O_2 reaction time course followed using single-wavelength detection at 450 and 350 nm. Approximately 80 μM Y257F-HPCA complex was mixed with ~500 μM O_2 at 4 °C and (A) pH 7.5 or (B) pH 5.5 (1 cm path length). The residuals from the fit are plotted on the same absorbance scale as the transient data but displaced for clarity.

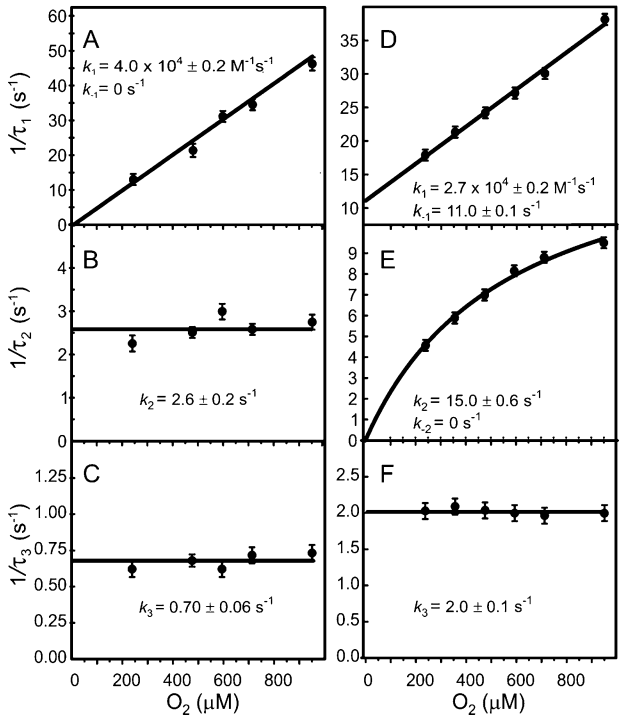

Figure 5. O_2 dependence of the three kinetically competent reciprocal relaxation times ($1/\tau$) from the Y257F-HPCA + O_2 reaction. The data were collected using single wavelength detection at 425 nm following the reaction of ~60−80 μM Y257F−HPCA complex with varying amounts of O_2 at 4 °C and pH 5.5 (panels A−C) or pH 7.5 (panels D−F).

The consequence of a fast reversible first step in the reaction is expected to be a hyperbolic plot for another of the $1/\tau$ vs O_2 plots, as observed in Figure 5E. The *y*-intercept of this plot is the reverse rate constant k_{-2} for the step following O_2 binding (zero in this case). The plot asymptotically approaches the sum of $k_2 + k_{-2}$, while the K_{app} for the plot is the K_d for the O_2 binding reaction (nonlinear fitting gives k_2 = 15.0 ± 0.6 s^{-1} and $K_d^{O_2}$ = 500 ± 40 μM). The irreversible nature of this step would uncouple the third reciprocal relaxation time from the others, so it would be expected to be independent of O_2 concentration and equal to the sum of the forward and reverse rate constants for the third step in the reaction, as observed ($k_3 + k_{-3}$ = 2 ± 0.1 s^{-1}) (Figure 5F). The amplitude for this uncoupled third phase monitored at 350 nm is much larger than those of the others, suggesting that the third step in the reaction is ring-cleavage. If this is the case, then the reaction is irreversible and k_{-3} = 0. The irreversible steps following O_2 association are presumably the explanation for the low observed K_m value for O_2 (Table 1) despite that rather high $K_d^{O_2}$ value for complex formation.

Returning to the pH 5.5 data, the occurrence of an initial irreversible O_2 binding step would uncouple $1/\tau_2$ and $1/\tau_3$ from O_2 concentration dependence, as observed in Figure 5B,C). This does not indicate *a priori* that $1/\tau_2$ and $1/\tau_3$ are uncoupled from each other, and they may not be if the second reaction step is reversible. However, our previous studies of intermediates in extradiol dioxygenase cycles have shown that the steps in their formation are generally well described as

Table 2. Reciprocal Relaxation Times and Amplitudes Obtained from Fitting Single Wavelength Data from the Y257F-HPCA + O_2 Reaction at One O_2 Concentration[a]

reciprocal relaxation time number	450 nm pH 5.5 s^{-1} (amp)	350 nm pH 5.5 s^{-1} (amp)	450 nm pH 7.5 s^{-1} (amp)	350 nm pH 7.5 s^{-1} (amp)
1	13 (0.09)	10 (−0.1)	21[b] (0.07)[c]	21 (0.017)
2	2.9 (−0.41)	2.9 (0.12)	5.5 (−0.40)	5.0 (0.18)
3	0.75 (0.30)	0.65 (−0.41)	1.8 (0.27)	2.2 (−0.91)
4	0.002 (−0.08)	0.002 (−0.08)	0.03 (−0.18)	0.03 (−0.25)

[a]Fitting to a 4 summed exponential equation by nonlinear regression using Pro Data viewer software available with Applied Photophysics SX series stopped-flow. 80 μM Y257F-HPCA complex was mixed with 500 μM O_2 at 4 °C and pH 7.5 (1 cm path length, 2 mm slit width). [b]The fitting error for all data in a single experimental run with at least 5 repeated trials is less than ±3%. For the experiment repeated using different enzyme batches over multiple days, the error is approximately ±10%. [c]The sign of an amplitude from exponential fitting is the opposite of the observed direction of change.

dx.doi.org/10.1021/bi301114x | *Biochemistry* 2012, 51, 8743−8754

irreversible; attack of an activated oxygen intermediate on substrate to form a covalent alkylperoxo species or subsequent breaking of the O−O bond are unlikely to be reversible processes.[8,12] Thus, it is likely that $1/\tau_2$ and $1/\tau_3$ are equal to rate constants of unique steps. This analysis does not indicate which rate constant is associated with which step, although it is likely that the order established by the pH 7.5 data is maintained (k_2 = 2.6 ± 0.2 s^{-1} and k_3 = 0.70 ± 0.06 s^{-1}). The assignment can be directly probed by analysis of the extinction coefficient of the chromophoric intermediate (see Discussion) or by directly trapping the intermediate for quantification using a technique such as Mössbauer spectroscopy, as described below.

Rate-Limiting Step. The rate constants for the reaction cycle steps that can be directly observed are all significantly greater than the k_{cat} value at both pH 7.5 and 5.5. These steps apparently encompass O_2 binding through formation of the product. Consequently, the rate limiting step must be either product release or a step in the substrate binding sequence or both.

Mössbauer Study of the Anaerobic Y257F-HPCA Complex. The anaerobic Y257F-HPCA complex ($Y257F_{ES}^{HPCA}$) exhibits well-resolved Mössbauer spectra in strong applied magnetic fields, B, a rather rare occurrence for the type of ligand environments afforded by ferrous sites with a 2-His-1-carboxylate facial triad ligand motif. Therefore, it is useful to extract zero field splitting (ZFS), magnetic hyperfine (^{57}Fe A-tensor) and electric field gradient (EFG) parameters from the data. Figures 6 and 7 show variable field, variable temperature Mössbauer spectra of $Y257F_{ES}^{HPCA}$. The zero field spectrum of Figure 6A exhibits a doublet with quadrupole splitting ΔE_Q = 3.19 mm/s and isomer shift δ = 1.12 mm/s, parameters typical

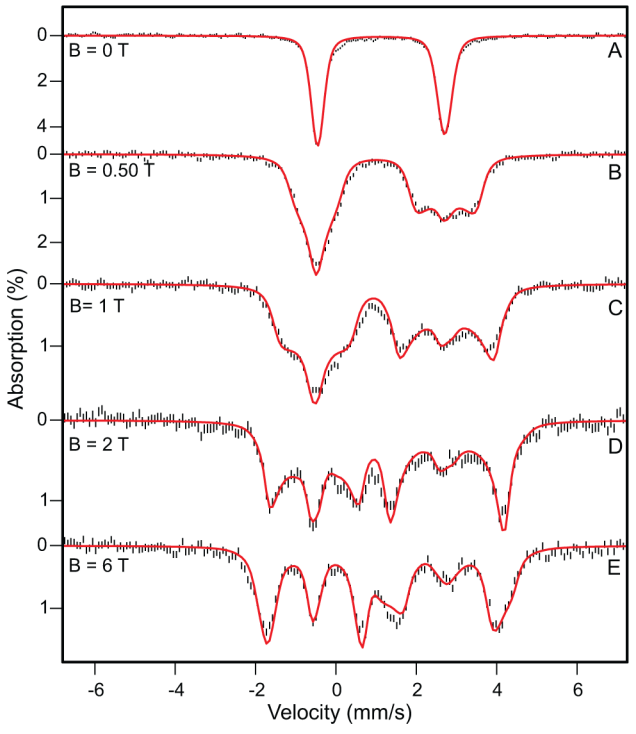

Figure 6. 4.2 K Mössbauer spectra of $Y257F_{ES}^{HPCA}$ recorded in parallel applied magnetic fields as indicated. The red curves are spectral simulations, in the slow relaxation limit of the electronic spin, based on the S = 2 Hamiltonian of eq 1 using the parameters listed in Table 3.

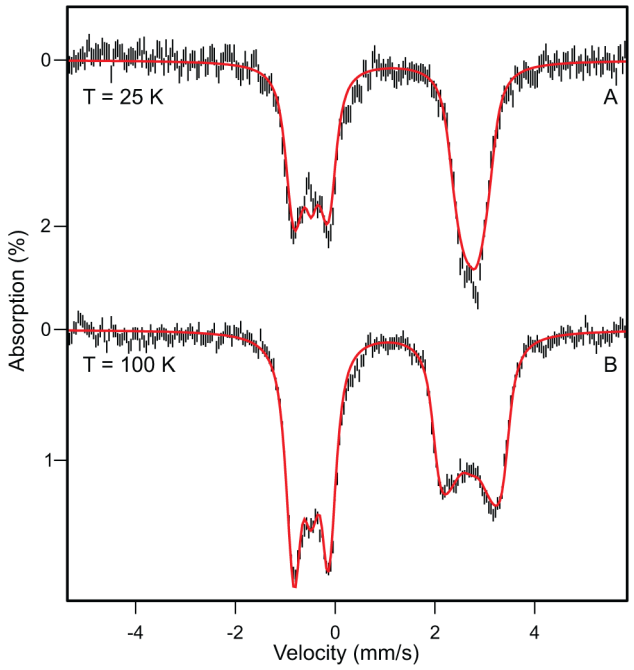

Figure 7. 6.0 T Mössbauer spectra of $Y257F_{ES}^{HPCA}$ recorded at the temperatures indicated on the left side of the figure. The red curves are spectral simulations, performed in the fast relaxation limit of the electronic spin, using the parameters of Table 3.

of high-spin Fe^{II}. $Y257F_{ES}^{HPCA}$ exhibits a single doublet, in contrast to the HPCA complexes formed with H200N and FeHPCD,[17] which exhibited, for reasons not yet understood, two species. The variable field spectra of $Y257F_{ES}^{HPCA}$ observed at 4.2 K reflect an S = 2 spin system for which the two lowest levels form a quasi-doublet with expectation values of the electronic spin, <**S**>, that are large in one particular direction (here z) and small in directions perpendicular to z. <**S**>, together with the ^{57}Fe magnetic hyperfine tensor, **A**, determines the internal magnetic field at the nucleus, $\mathbf{B}_{int} = -\langle\mathbf{S}\rangle\cdot\mathbf{A}/g_n\beta_n$, which in turn determines the observed magnetic splitting. We have analyzed the spectra of Figures 6 and 7 in the framework of the commonly used S = 2 spin Hamiltonian:

$$\mathcal{H} = D\left[S_z^2 - 2 + \left(\frac{E}{D}\right)(S_x^2 - S_y^2)\right] + \beta\vec{S}\cdot\hat{g}\cdot\vec{B} + \vec{S}\cdot\hat{A}\cdot\vec{I} - g_n\beta_n\vec{B}\cdot\vec{I} + \frac{eQV_{z'z'}}{12}\left[3I_{z'}^2 - \frac{15}{4} + \eta(I_{x'}^2 - I_{y'}^2)\right] \quad (1)$$

The traceless ZFS tensor (parameters D and E) defines the main molecular frame, (x, y, z). The quadrupole interaction (the last term in eq 1) is written in its conventional form in the frame (x', y', z'). The method of analyzing the spectra follows that described by Zimmermann et al. for protocatechuate 3,4 dioxygenase.[22] Our major conclusions are summarized in the following. The ZFS tensor of Y257F-HPCA is nearly rhombic, E/D = 0.32. For perfect rhombicity, namely, E/D = 1/3, the three t_{2g}-derived orbital states would be equally spaced with respect to each other (provided they have the same covalency).[23] The two lowest spin levels of $Y257F_{ES}^{HPCA}$ have M_S = ± 2 heritage (i.e., they would have the exact M_S = ± 2 label in the limit E/D = 0). In moderate applied fields, the induced magnetic hyperfine interactions of the spectra of Figure 6B−D depends on the splitting Δ of the "M_S = ± 2"

dx.doi.org/10.1021/bi301114x | Biochemistry 2012, 51, 8743−8754

doublet and not on D and E/D separately, where Δ is given by[22]

$$\Delta = 2D[(1 + 3(E/D)^2)^{1/2} - 1] \quad (2)$$

Analysis of the spectra in Figure 6B–D showed that $Y257F_{ES}^{HPCA}$ has $\Delta \cong 3.2$ cm^{-1}. This Δ value is much too large for observation of integer spin EPR signals at either X- or Q-band ($h\upsilon = 0.3$ cm^{-1} at X-band). Further analysis revealed that the EFG tensor of $Y257F_{ES}^{HPCA}$ is quite axial ($\eta = (V_{x'x'} - V_{y'y'})/V_{z'z'} = 0.20$), that its largest component, $V_{z'z'}$, is positive (hence $\Delta E_Q > 0$), and that z' makes an angle $\beta_{EFG} \approx 27°$ relative to z. The stated properties are readily extracted from the spectra of Figure 6B–D. The high-energy (right) features of the spectra of Figure 6B,C depends on g_zA_z. However, the right-hand features of Figure 6D depend only on A_z (for the quoted value of Δ the expectation value $<S_z>$ saturates at $<S_z> = -2$ independent of g_z), which allowed us to determine $A_z/g_n\beta_n = -6.3$ T. Above 20 K the electronic spin system is in the fast relaxation regime. The 25 K spectrum shown in Figure 7A is reasonably sensitive to D but depends only weakly on E/D. This behavior allowed for fitting of the 25 K spectrum to obtain $D = -11.2$ cm^{-1} which, using the expression for Δ, yielded $E/D = 0.32$.

The simulations shown in Figures 6 and 7 represent the data very well. The spin Hamiltonian parameters of Table 3 will be a useful spectroscopic benchmark for density functional calculations based on the X-ray structure of $Y257F_{ES}^{HPCA}$ (see accompanying report). The solution presented in Table 3 is not unique. We have made many attempts to fit the spectra and have found that all reasonable solutions share the following features: D is confined to (9–11) cm^{-1} and, roughly, $0.31 < E/D < 0.36$. β_{EFG} may vary between 20 and 35°, and β_A is between 3 and 10° ($\beta_A = 0$ did not produce good fits). The observation that the EFG and A-tensors have different principal axis systems suggests that the A-tensor has substantial orbital contributions; as the latter are proportional to $(g_i - 2)$, it follows that the g-values cannot be 2.00, as we have arbitrarily assumed. The orbital contributions to **A** are expected to be diagonal in (x, y, z), whereas the spin-dipolar contribution to **A** is expected to be diagonal in (x', y', z'), the principal axis system of the EFG tensor. The combination of the orbital and spin dipolar parts determines the principal axis frame of the A-tensor. The software package WMOSS allows group fits to *theoretical* spectra. Thus, if quantum chemical calculations suggest different solutions, researchers can use the solution given here to explore whether particular parameter sets are compatible with the data.

Density functional calculations, combined with a ligand field approach, will relate the spin Hamiltonian parameters to molecular coordinates and delineate the orbitals available for interaction with O_2; such studies are in progress. While these calculations are beyond the scope of the present work, the spectra collected here are useful in judging the Mössbauer spectra of $Y257F_{Int1}^{HPCA}$ and $Y257F_{Int2}^{HPCA}$, presented next.

Table 3. $S = 2$ Spin Hamiltonian Parameters of Y257F-HPCA Evaluated Using eq 1

$D = -11.2$ cm^{-1}	$A_x/g_e\beta_n = -22$ T	$\Delta E_Q = +3.19$ mm/s
$E/D = 0.32$	$A_y/g_e\beta_n \sim -29$ T	$\eta = 0.20$
$g_x = 2.00$[a]	$A_z/g_e\beta_n = -6.3$ T	$(\alpha\beta\gamma)_{EFG}$[b] = (160, 27, 0)°
$g_y = 2.00$		$(\alpha\beta\gamma)_A$[b] = (98, 6.5,76)°
$g_z = 2.00$	$\delta = 1.12$ mm/s	

[a] g-values were fixed to $g = 2.00$. [b] $(\alpha\beta\gamma)_{EFG}$ and $(\alpha\beta\gamma)_A$ are the Euler angles that rotate the EFG- and A-tensor into (x, y, z). The simulations are more sensitive to β than to α and γ.

Mössbauer Spectra of $Y257F_{Int1}^{HPCA}$ and $Y257F_{Int2}^{HPCA}$. Figure 8 shows 4.2 K Mössbauer spectra recorded for $B = 0$

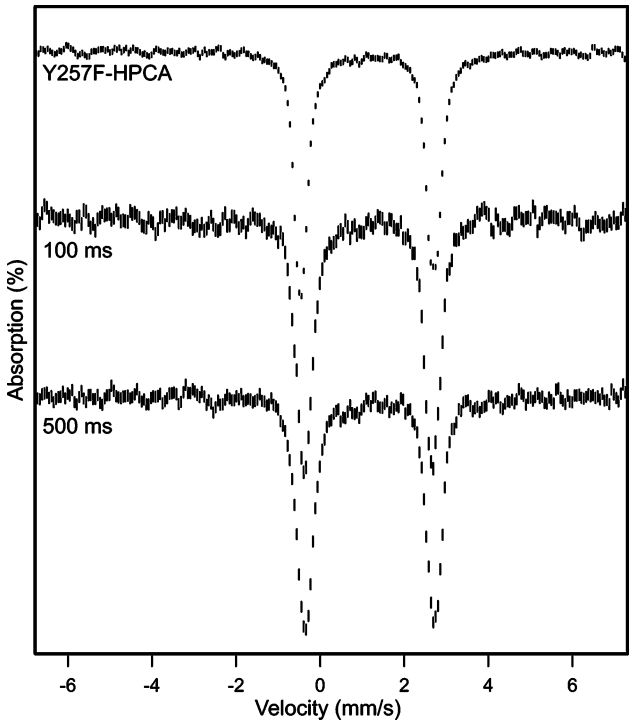

Figure 8. Zero field 4.2 K Mössbauer spectra of $Y257F_{ES}^{HPCA}$, $Y257F_{Int1}^{HPCA}$ (100 ms sample) and $Y257F_{Int2}^{HPCA}$ (500 ms sample). Quadrupole splittings and isomer shifts are $\Delta E_Q = 3.02(3)$ mm/s and $\delta = 1.15(2)$ mm/s for $Y257F_{Int1}^{HPCA}$ and $\Delta E_Q = 3.08(3)$ mm/s and $\delta = 1.18(2)$ mm/s for $Y257F_{Int2}^{HPCA}$ (see text).

of $Y257F_{Int1}^{HPCA}$ and $Y257F_{Int2}^{HPCA}$ formed at pH 6.0. The sample for $Y257F_{Int1}^{HPCA}$ was rapidly quenched 100 ms after mixing with O_2. The kinetic data suggests that this sample should contain 60% $Y257F_{Int1}^{HPCA}$, 20% $Y257F_{Int2}^{HPCA}$ and 20% $Y257F_{ES}^{HPCA}$ (see Discussion). The sample for $Y257F_{Int2}^{HPCA}$ was quenched at 500 ms and, according to the kinetic data, should contain 60% $Y257F_{Int2}^{HPCA}$, 20% $Y257F_{Int1}^{HPCA}$ and 20% Y257F-product ($Y257F_{Prod}^{HPCA}$). Neither sample exhibited an EPR spectrum in either perpendicular or parallel mode. It can be seen that the spectra of the two samples are essentially the same, and moreover, the spectra are close to those seen for the $Y257F_{ES}^{HPCA}$ and $Y257F_{Prod}^{HPCA}$; zero field spectra for $Y257F_{ES}^{HPCA}$ and $Y257F_{Prod}^{HPCA}$, $Y257F_{Int1}^{HPCA}$ and $Y257F_{Int2}^{HPCA}$ are shown in Figure S3. Clearly, the iron sites of $Y257F_{Int1}^{HPCA}$ and $Y257F_{Int2}^{HPCA}$ are high-spin ferrous, in stark contrast to the Fe^{III} – radical intermediates observed for the early oxy-intermediates of the H200N variant.[16,17] In order to get the best possible ΔE_Q and δ values for $Y257F_{Int1}^{HPCA}$ and $Y257F_{Int2}^{HPCA}$ the contributions of $Y257F_{ES}^{HPCA}$ and $Y257F_{Prod}^{HPCA}$ were subtracted from the spectra and then the remaining spectra were combined such that the contribution of either $Y257F_{Int1}^{HPCA}$ or $Y257F_{Int2}^{HPCA}$ canceled. In this way, we found $\Delta E_Q = 3.02(3)$ mm/s and $\delta = 1.15(2)$ mm/s for $Y257F_{Int1}^{HPCA}$ and $\Delta E_Q = 3.08(3)$ mm/s and $\delta = 1.18(2)$ mm/s for $Y257F_{Int2}^{HPCA}$.

dx.doi.org/10.1021/bi301114x | *Biochemistry* 2012, 51, 8743–8754

Figure 9 shows 2.0 T spectra of Y257F$_{Int1}^{HPCA}$ (black hash marks) and Y257F$_{Int2}^{HPCA}$ (blue) samples recorded at 4.2 K. For comparison, we show the theoretical curve (red) of the Y257F$_{ES}^{HPCA}$ complex. It can be seen that the 2T spectra of Y257F$_{Int1}^{HPCA}$ and Y257F$_{Int2}^{HPCA}$ are indistinguishable within the noise, and that both differ from the spectrum of Y257F$_{ES}^{HPCA}$. Subtraction of the spectrum represented by the red curve from the 2T spectrum of Y257F$_{Int1}^{HPCA}$ showed that the 100 ms sample could have no more than 15% contribution to the total iron from Y257F$_{ES}^{HPCA}$. Likewise, subtraction of the zero field spectrum of Y257F$_{Prod}^{HPCA}$ from the corresponding spectrum of the 500 ms sample showed the end complex can account for no more than 20% of total iron in the 500 ms sample.

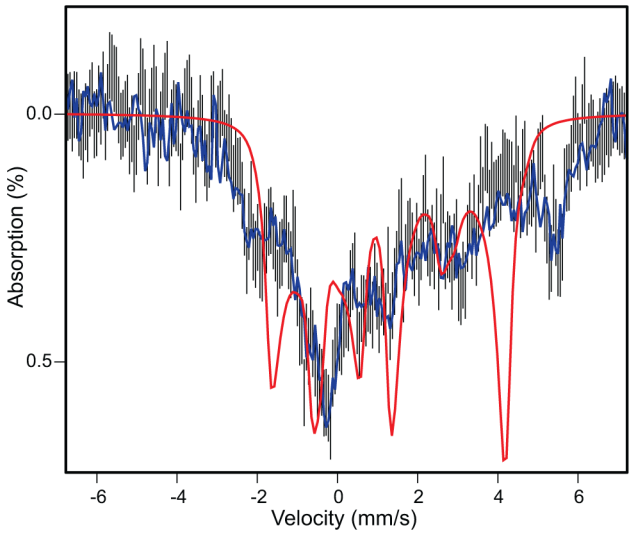

Figure 9. 2.0 T Mössbauer spectra of Y257F$_{Int1}^{HPCA}$ (black hashed) and Y257F$_{Int2}^{HPCA}$ (blue) recorded at 4.2 K. For comparison is shown the spectral simulation for the enzyme substrate complex, Y257F-HPCA (red, same curve as in Figure 6D).

The reader may wonder why the ΔE_Q values of Y257F, Y257F$_{ES}^{HPCA}$, Y257F$_{Int1}^{HPCA}$ Y257F$_{Int2}^{HPCA}$ and Y257F$_{Prod}^{HPCA}$ are the same within 6%. The present complexes have a distorted octahedral symmetry for which the three lowest states are combinations of mainly d_{xy}, d_{yz}, and d_{xz} orbitals. It has been shown that any linear combination of these three orbitals (the $^5T_2$ approximation) yields the same ΔE_Q at 4.2 K as long as there are no major changes in covalency.[24] As the states observed here present us with various FeO_5N coordinations, the small variability in ΔE_Q is not surprising.

DISCUSSION

The results described here show that Tyr257 plays an important role in efficient catalysis at several points in the catalytic cycle of FeHPCD. Structural studies indicate that it has two different types of interactions with the substrate.[2,3,6] First, there is a van der Waals interaction between the Tyr-OH and the C2 carbon of the substrate forcing a slight global deformation to the aromatic ring. Second, the Tyr-OH forms a hydrogen bond to the deprotonated substrate C2−O$^-$ in both the anaerobic enzyme substrate complex and the FeHPCD$_{Int1}^{4NC}$ intermediate (Figure 1). The second interaction causes a substantial localized distortion in the normally planar ring. This work complements earlier studies in which the roles of His200 and the nature of its interaction with the second iron-bound substrate, O_2, were examined.[12,16,17,25] These studies support the hypothesis that the two substrates are connected electronically through the iron and that the transfer of electron density from the catecholic substrate to O_2 is the basis for oxygen activation in this system. The current studies show that the second sphere residues of the iron, specifically His200 and Tyr257, must also work in concert to make the O_2 activation process efficient and specific. Newly recognized aspects of this complex collaboration for catalysis are discussed here.

Kinetic Model for Catalysis. The rate constants assigned for the single turnover reactions at pH 7.5 and 5.5 are shown in Scheme 2, panels A and B, respectively. Figure 10 shows a

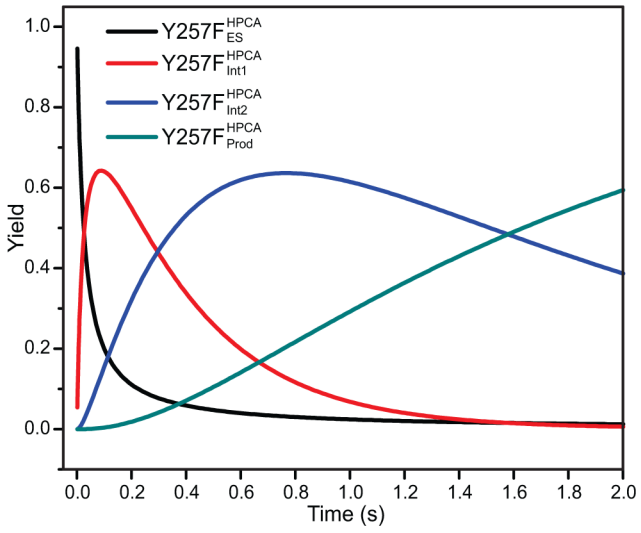

Figure 10. Simulation of expected time-dependent relative yields for reaction intermediates from the Y257F-HPCA + O_2 reaction at pH 5.5 for the model shown in Scheme 2B.

Scheme 2. Kinetic Models for Species Occurring in the Y257F-HPCA + O_2 Single-Turnover Reaction[a]

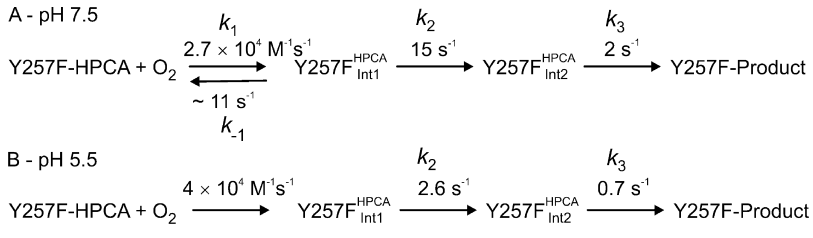

[a]Rate constants are as determined from kinetic analysis of the Y257F-HPCA + O_2 reaction at pH 7.5 (Model A) and pH 5.5 (Model B).

dx.doi.org/10.1021/bi301114x | Biochemistry 2012, 51, 8743−8754

Table 4. Intermediates Formed by FeHPCD and Its Variants with HPCA and Alternative Substrates

intermediate[a]	Fe ox state (Mössbauer)	optical spectrum ε, M^{-1} cm^{-1}	EPR spectrum	reversible O_2 binding	assignment	ref
$FeHPCD_{Int1}^{HPCA}$	Fe^{II}	no	no	no	Fe^{II}-alkylperoxo	17
$H200N_{Int1}^{HPCA}$	Fe^{III} spin-coupled	yes HPCA-SQ $\varepsilon_{395} \cong 3200$ $\varepsilon_{610} \cong 1100$	yes $S = 2$ ES[b]	no	HPCA SQ-Fe^{III}-(H) peroxo	17
$H200N_{Int2}^{HPCA}$	Fe^{II}	no	no	no	Fe^{II}-alkylperoxo	17
$H200N_{Int1}^{4NC}$	Fe^{III} spin-coupled	yes 4NC $\varepsilon_{506} \cong 10000$ $\varepsilon_{630} \cong 1200$	yes $S = 2$ GS[b]	yes	4NC-Fe^{III}–$O_2^{\bullet-}$	16
$H200N_{Int2}^{4NC}$	Fe^{III} spin-coupled	yes 4NC-SQ $\varepsilon_{405} \cong 15000$ $\varepsilon_{675} \cong 1000$	yes $S = 2$ ES	N/A[b]	4NC SQ-Fe^{III}-(H)peroxo	16
$Y257F_{Int1}^{HPCA}$	Fe^{II}	no	no	yes	HPCA-Fe^{II}–O_2	this work
$Y257F_{Int2}^{HPCA}$	Fe^{II}	yes $\varepsilon_{425} \cong 10500$	no	N/A[b]	HPCA Q-Fe^{II}-(H)peroxo	this work

[a] $FeHPCD_{Int1}^{HPCA}$, first intermediate observed after mixing FeHPCD-HPCA with O_2; $H200N_{Int1}^{HPCA}$ and $H200N_{Int2}^{HPCA}$, first and second intermediates observed after mixing H200N-HPCA with O_2; $H200N_{Int1}^{4NC}$ and $H200N_{Int2}^{4NC}$ first and second intermediates observed after mixing H200N-4NC with O_2
[b] Abbreviations: ES = excited state; GS = ground state; N/A = not applicable.

numerical integration simulation of the single turnover reaction of Y257F-HPCA + O_2 at pH 5.5 for the model shown in Scheme 2B. The simulation predicts that $Y257F_{Int1}^{HPCA}$ will accumulate to ~64% at 90 ms, and $Y257F_{Int2}^{HPCA}$ will build to ~63% at 700 ms. The simulation for the reaction at pH 7.5 predicts an accumulation of $Y257F_{Int1}^{HPCA}$ of ~30% at 50 ms, while that of $Y257F_{Int2}^{HPCA}$ is computed to be ~55% at 250 ms (simulation not shown). These values together with the known total enzyme concentration can be used to predict the extinction coefficient of $Y257F_{Int2}^{HPCA}$ of ε_{425} =10 500 M^{-1} cm^{-1} at each pH value. The values predicted by Model B at pH 5.5 for the intermediate concentrations are similar to those observed in RFQ/Mössbauer samples from a reaction time course at pH 6.0 (Figure 8), supporting the order for the rate constants associated with the second and third steps shown in Scheme 2 (enzyme precipitation at high concentration prevented making pH 5.5 Mössbauer samples).

Chemical Nature of $Y257F_{Int1}^{HPCA}$. $Y257F_{Int1}^{HPCA}$ forms in a second-order reaction between Y257F-HPCA and O_2, so it is an oxygen complex of some sort. However, it differs from each of the oxygen complexes found thus far for FeHPCD and its variants as summarized in Table 4. For example, $Y257F_{Int1}^{HPCA}$ closely resembles $FeHPCD_{Int1}^{HPCA}$ in most of its characteristics, but these intermediates are clearly quite different because only $Y257F_{Int1}^{HPCA}$ exhibits an O_2 concentration dependence for its formation rate constant. Consequently, $Y257F_{Int1}^{HPCA}$ must represent a species occurring as O_2 binds, while we have proposed that $FeHPCD_{Int1}^{HPCA}$ is a species occurring after irreversible oxygen attack on the substrate. [17] $Y257F_{Int1}^{HPCA}$ could, in principle, be the $SQ^{\bullet}$-Fe^{II}–$O_2^{\bullet-}$ species postulated to be the reactive oxygen-activated species and observed *in crystallo* when a crystal of FeHPCD-4NC is exposed to O_2.[6] However, it is illustrated below that the electronic transitions which give rise to the $SQ^{\bullet}$ chromophore are easily detected and not greatly perturbed when the $SQ^{\bullet}$ ligand is exchange coupled to a high-spin Fe^{III}-(H)peroxo site. This is likely to also be the case for a $SQ^{\bullet}$ ligand bound to an Fe^{II}–$O_2^{\bullet-}$ site, but there is no precedent in solution for this state to the best of our knowledge. Consequently, the lack of a strong chromophore from $Y257F_{Int1}^{HPCA}$ suggests that this intermediate does not contain a semiquinone or quinone form of the substrate. Since Mössbauer data show that $Y257F_{Int1}^{HPCA}$ contains only Fe^{II}, the lack of a bound $SQ^{\bullet}$ or quinone suggests that the bound oxygen must remain close to the O_2 oxidation state. This would not be expected to be a strong bond, which is in accord with the weak affinity observed here for the complex at pH 7.5 (see below for a discussion of the complex at pH 5.5). It is also possible that O_2 is bound in the active site, but not to the iron (In this case, however, there must be some adjustment in the iron coordination as the Mössbauer spectra of $Y257F_{Int1}^{HPCA}$ differ from those of Y257F-HPCA as shown in Figure 9). This type of complex appears to be an intermediate in the O_2 binding process in FeHPCD and other dioxygenases based on previous transient kinetic studies.[8,26,27] We propose that $Y257F_{Int1}^{HPCA}$ is most likely an HPCA-Fe^{II}-O_2 complex with minor electron transfer or spin delocalization to the oxygen. The relevance of this conclusion to the role of Tyr257 is discussed below.

Chemical Nature of $Y257F_{Int2}^{HPCA}$. In contrast to $Y257F_{Int1}^{HPCA}$, $Y257F_{Int2}^{HPCA}$ exhibits a relatively intense chromophore at 425 nm and possibly a weak feature near 325 nm. The λ_{max} and intensity of this chromophore are consistent with the spectra observed in the UV–vis region from unbound quinones or semiquinones, albeit with a slightly larger extinction coefficient.[17] In the absence of FeHPCD, incubation of HPCA with a high potential quinone results in an unbound HPCA-$SQ^{\bullet}$ exhibiting a very similar long wavelength spectrum to that observed for $H200N_{Int1}^{HPCA}$ (Figure 11, λ_{max} near 610 for $H200N_{Int1}^{HPCA}$ and 645 nm for HPCA-$SQ^{\bullet}$),[17] suggesting that the electronic transitions which give rise to the $SQ^{\bullet}$ chromophore are retained when the $SQ^{\bullet}$ ligand is exchange coupled to a high-spin Fe^{III}-(H)peroxo site. This is likely to also be true for a $SQ^{\bullet}$-Fe^{II}-$O_2^{\bullet-}$

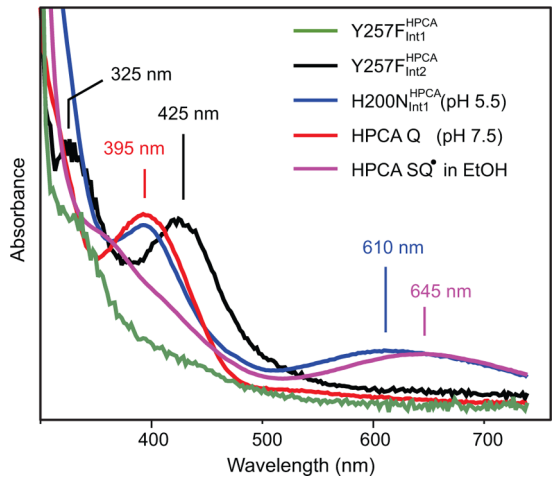

Figure 11. Comparison of UV–vis spectra of unbound HPCA quinone and HPCA semiquinone to those of $Y257F_{Int1}^{HPCA}$, $Y257F_{Int2}^{HPCA}$ and $H200N_{Int1}^{HPCA}$. The spectra of $Y257F_{Int1}^{HPCA}$ and $Y257F_{Int2}^{HPCA}$ are derived from the time course of Figure 3. HPCA quinone and HPCA semiquinone were synthesized as described in Experimental Procedures. The spectra are scaled arbitrarily to facilitate comparison of UV–vis features.

dx.doi.org/10.1021/bi301114x | *Biochemistry* 2012, 51, 8743–8754

site, since the origin of the semiquinone chromophore is not charge transfer to the iron.

The UV−vis spectrum of $Y257F_{Int2}^{HPCA}$ is missing the low energy UV−vis feature associated with the HPCA-SQ•, but it does have a feature similar to that observed for the unbound HPCA-Q (Figure 11, λ_{max} near 425 nm for $Y257F_{Int2}^{HPCA}$ and 395 nm for unbound HPCA-Q). On the basis of this spectrum, $Y257F_{Int2}^{HPCA}$ is unlikely to contain a HPCA SQ•. Mössbauer spectra from a sample expected to contain >60% $Y257F_{Int2}^{HPCA}$ shows that only Fe^{II} species are present. The absence of Fe^{III} species, the lack of a low-energy band, and the presence of an intense feature near 425 nm suggest that $Y257F_{Int2}^{HPCA}$ is most likely a HPCA-Q-Fe^{II}-(H)peroxo complex.

Origin of Rate Constant Decreases in Reaction Cycle Steps − Mechanistic Significance. The rate constants for intermediate conversion in the catalytic cycle are affected in similar ways by the Y257F mutation as by the use of 4NC as the substrate. We have proposed that 4NC slows the reaction because the electron withdrawing nitro substituent makes electron transfer through the Fe^{II} to the O_2 less favorable.[8,11,12] This is dramatically observed in the H200N-4NC reaction with O_2 where the 4NC-Fe^{III}-$O_2^{\bullet-}$ species persists for hundreds of seconds without attacking the 4NC.[16] In the case of HPCA, the electron donating inductive effects of the para substituent will make it much more favorable to donate an electron through the iron to the O_2, leading to rapid, nearly irreversible binding. The effect of this putative electron transfer will be to give the substrate semiquinone character that would facilitate subsequent attack by the superoxo species formed in the process. However, a radical semiquinone will normally form by delocalizing the unpaired spin on the ring, which would cause the ring to remain essentially planar. Moreover, no position would be preferentially activated for attack by the superoxide, so specificity would result solely from orientation of the superoxo moiety. Stabilization of the HPCA C2−O^- below the plane of the ring by interaction with Tyr257 would serve to not only promote the formation of the semiquinone, and thus electron transfer, but also to localize the radical on HPCA C2. This would activate this position for superoxide attack, thereby accelerating the reaction. It is possible that without this additional stabilization, electron transfer between the substrates does not readily occur, leading to slow kinetics for the same reasons just described for the 4NC reaction.

The natures of $Y257F_{Int1}^{HPCA}$ and $Y257F_{Int2}^{HPCA}$ appear to support the proposal that the rate of electron transfer between substrates is slowed. The discussion above suggests that no electron has transferred from the substrate in $Y257F_{Int1}^{HPCA}$, while in $Y257F_{Int2}^{HPCA}$ most likely two electrons have transferred without attack on the substrate by a putative intermediate superoxo species as occurs in the reaction cycle of the WT enzyme. It may be that without the localized radical and ring distortion caused by Tyr257, attack on the ring is much less favorable. It remains unclear whether the attacking species is superoxo or (hydro)peroxo in the wild type enzyme with HPCA as the substrate. While it appears from the current results that the (hydro)peroxo intermediate can go forward to attack the quinone form of the aromatic substrate, this reaction is slow relative to the normal rate of formation of the alkylperoxo intermediate. One possibility is that the electrons from substrate are transferred one at a time, normally leading to a reactive substrate and oxygen radical pair after the first electron is transferred. If the reactivity of this pair is decreased due to lack of stabilization by Tyr257, then there is time for transfer of the second electron to form the quinone and (hydro)peroxo pair bound to the Fe^{II}.

Basis for pH Effects on O_2 Binding. The binding of O_2 to the iron of FeHPCD is a complex process that is carefully regulated to ensure specificity. The current and several past studies show that substrate must bind first to provide the electrons needed to stabilize the Fe−O_2 bond and perhaps to facilitate the release of solvent that blocks the O_2 binding site in the resting enzyme.[28−31] In the absence of Tyr257, we hypothesize that the supply of electrons to stabilize the Fe−O_2 bond will be compromised, causing the binding process to be slow and reversible. One way the enzyme can counter the reversibility is to protonate His200 which is in hydrogen bonding and charge interaction range of the bound O_2 (Figure 1). In particular, the new positive charge gained by protonating His200 at low pH would stabilize the $O_2^{\bullet-}$ character as O_2 binds to the iron. This would not necessarily make the binding process more rapid, but it might serve to slow oxygen release leading to the observed high O_2 affinity.

Roles of Tyr257 in Other Reaction Cycle Steps. The results indicate that the slowest step in the reaction of Y257F is shifted from product formation to either product release or substrate binding. This suggests that Tyr257 may play a role in one or both of these processes. In another branch of the extradiol dioxygenase family typified by *Sphingomonas paucimobilis* SYK-6 protocatechuate 4,5-dioxygenase (LigAB) or *E. coli* 2,3-dihydroxyphenylpropionate 1,2-dioxygenase (MhpB), a histidine is sometimes present in place of Tyr257.[32] Mutagenesis and kinetic studies of MhpB indicate that this histidine may play a role as a base catalyst by promoting deprotonation of the substrate during binding with transfer back to the lactone intermediate during ring-opening.[33] The structural studies presented in the accompanying report suggest that Tyr257 is not involved in active site interactions that would stabilize a deprotonated form, and thus it is unlikely to act as an active site base.[2] However, it does participate in key hydrogen bonding and van der Waals interactions with substrate that would favor the anionic form of the substrate C2-hydroxyl. Thus, it may accomplish some of the mechanistically relevant roles attributed to the MhpB histidine through a different strategy. These interactions are absent in Y257F, and this may account for the decreased rate of steps in the substrate binding and/or product release processes.

■ CONCLUSION

For the reaction of the WT FeHPCD, the oxygen binding, activation, and reaction steps to form the alkylperoxo intermediate of the reaction cycle are complete within the dead time of the stopped flow instrument at 4 °C (~1 ms). In contrast, these steps in the Y257F variant require well over 100 ms to complete. The >100-fold decrease in the observed rate (and rate constants) shows that Tyr257 plays a key role in aiding the ring attack/oxygen insertion steps. The catalytic process does proceed in the absence of Tyr257, encompassing the putative HPCA-Fe^{II}-O_2 and HPCA quinone-Fe^{II}-(H)-peroxo intermediates described here, but the decreased rates suggest that these intermediates are not optimized for the most efficient catalytic process.

■ ASSOCIATED CONTENT

Supporting Information

Supporting results, Figures S1−S3. This material is available free of charge via the Internet at http://pubs.acs.org.

dx.doi.org/10.1021/bi301114x | *Biochemistry* 2012, 51, 8743−8754

AUTHOR INFORMATION

Corresponding Author

*(E.M.) Address: Department of Chemistry, Carnegie Mellon University, 4400 Fifth Ave., Pittsburgh, PA 15213; e-mail, EMunck@cmu.edu; phone, (412) 268-5058. (J.D.L.) Address: Department of Biochemistry, Molecular Biology, and Biophysics, 6-155 Jackson Hall, University of Minnesota, 321 Church St. SE, Minneapolis, MN 55455; phone, (612) 625-6454; fax, (612) 624-5121; e-mail, Lipsc001@umn.edu.

Funding

This work is supported by National Institutes of Health Grant GM 24689 (to J.D.L.), NSF Grant CHE-1012485 (to E.M.), and Graduate Traineeship GM08700 (to M.M.M.).

Notes

The authors declare no competing financial interest.

ABBREVIATIONS USED

FeHPCD, recombinant homoprotocatechuate 2,3-dioxygenase from *Brevibacterium fuscum*; WT, wild type or unmodified FeHPCD; H200N, His200Asn variant of FeHPCD; Y257F, Tyr257Phe variant of FeHPCD; HPCA, homoprotocatechuate or 3,4-dihydroxyphenylacetate or 4-carboxymethyl catechol; 4NC, 4-nitrocatechol; $FeHPCD^{HPCA}_{ES}$, anaerobic FeHPCD-HPCA complex; $Y257F^{HPCA}_{ES}$, anaerobic Y257F-HPCA complex; $Y257F^{HPCA}_{Int1}$ and $Y257F^{HPCA}_{Int2}$, novel intermediates observed in the Y257F-HPCA + O_2 reaction; Q, quinone; $SQ^{\bullet}$, semiquinone; EPR, electron paramagnetic resonance; RFQ, rapid-freeze-quench; ICP-OES, inductively coupled plasma optical emission spectroscopy; LMCT, ligand to metal charge transfer transition

REFERENCES

(1) Miller, M. A., and Lipscomb, J. D. (1996) Homoprotocatechuate 2,3-dioxygenase from *Brevibacterium fuscum* - A dioxygenase with catalase activity. *J. Biol. Chem. 271*, 5524−5535.

(2) Kovaleva, E. G. Lipscomb, J. D. Structural basis for the role of tyrosine 257 of homoprotocatechuate 2,3-dioxygenase in substrate and oxygen activation. *Biochemistry* 2012 *51*, DOI: 10.1021/bi301115c.

(3) Vetting, M. W., Wackett, L. P., Que, L., Jr., Lipscomb, J. D., and Ohlendorf, D. H. (2004) Crystallographic comparison of manganese- and iron-dependent homoprotocatechuate 2,3-dioxygenases. *J. Bacteriol. 186*, 1945−1958.

(4) Han, S., Eltis, L. D., Timmis, K. N., Muchmore, S. W., and Bolin, J. T. (1995) Crystal structure of the biphenyl-cleaving extradiol dioxygenase from a PCB-degrading pseudomonad. *Science 270*, 976−980.

(5) Senda, T., Sugiyama, K., Narita, H., Yamamoto, T., Kimbara, K., Fukuda, M., Sato, M., Yano, K., and Mitsui, Y. (1996) Three-dimensional structures of free form and two substrate complexes of an extradiol ring-cleavage type dioxygenase, the BphC enzyme from *Pseudomonas sp*. strain KKS102. *J. Mol. Biol. 255*, 735−752.

(6) Kovaleva, E. G., and Lipscomb, J. D. (2007) Crystal structures of Fe^{2+} dioxygenase superoxo, alkylperoxo, and bound product intermediates. *Science 316*, 453−457.

(7) Hegg, E. L., and Que, L. (1997) The 2-His-1-carboxylate facial triad: An emerging structural motif in mononuclear non-heme iron(II) enzymes. *Eur. J. Biochem. 250*, 625−629.

(8) Groce, S. L., Miller-Rodeberg, M. A., and Lipscomb, J. D. (2004) Single-turnover kinetics of homoprotocatechuate 2,3-dioxygenase. *Biochemistry 43*, 15141−15153.

(9) Vaillancourt, F. H., Barbosa, C. J., Spiro, T. G., Bolin, J. T., Blades, M. W., Turner, R. F. B., and Eltis, L. D. (2002) Definitive evidence for monoanionic binding of 2,3-dihydroxybiphenyl to 2,3-dihydroxybiphenyl 1,2-dioxygenase from UV resonance Raman spectroscopy, UV/vis absorption spectroscopy, and crystallography. *J. Am. Chem. Soc. 124*, 2485−2496.

(10) Arciero, D. M., and Lipscomb, J. D. (1986) Binding of ^{17}O-labeled substrate and inhibitors to protocatechuate 4,5-dioxygenase-nitrosyl complex. Evidence for direct substrate binding to the active site Fe^{2+} of extradiol dioxygenases. *J. Biol. Chem. 261*, 2170−2178.

(11) Lipscomb, J. D. (2008) Mechanism of extradiol aromatic ring-cleaving dioxygenases. *Curr. Opin. Struct. Biol. 18*, 644−649.

(12) Groce, S. L., and Lipscomb, J. D. (2005) Aromatic ring cleavage by homoprotocatechuate 2,3-dioxygenase: Role of His200 in the kinetics of interconversion of reaction cycle intermediates. *Biochemistry 44*, 7175−7188.

(13) Vaillancourt, F. H., Bolin, J. T., and Eltis, L. D. (2006) The ins and outs of ring-cleaving dioxygenases. *Crit. Rev. Biochem. Mol. Biol. 41*, 241−267.

(14) Bugg, T. D. H. (2011) Non-heme iron-dependent dioxygenases: Mechanism and structure, In *Iron-Containing Enzymes: Versatile Catalysts of Hydroxylation Reactions in Nature* (de Visser, S. P., Kumar, D., Eds.) pp 42−66, The Royal Society of Chemistry, Cambridge, UK.

(15) Kovaleva, E. G., and Lipscomb, J. D. (2008) Intermediate in the O-O bond cleavage reaction of an extradiol dioxygenase. *Biochemistry 47*, 11168−11170.

(16) Mbughuni, M. M., Chakrabarti, M., Hayden, J. A., Bominaar, E. L., Hendrich, M. P., Münck, E., and Lipscomb, J. D. (2010) Trapping and spectroscopic characterization of an Fe^{III}-superoxo intermediate from a nonheme mononuclear iron-containing enzyme. *Proc. Natl. Acad. Sci. U. S. A. 107*, 16788−16793.

(17) Mbughuni, M. M., Chakrabarti, M., Hayden, J. A., Meier, K. K., Dalluge, J. J., Hendrich, M. P., Münck, E., and Lipscomb, J. D. (2011) Oxy-intermediates of homoprotocatechuate 2,3-dioxygenase: Facile electron transfer between substrates. *Biochemistry 50*, 10262−10274.

(18) Lee, S. K., Nesheim, J. C., and Lipscomb, J. D. (1993) Transient intermediates of the methane monooxygenase catalytic cycle. *J. Biol. Chem. 268*, 21569−21577.

(19) Münck, E. (2000) Aspects of ^{57}Fe Mössbauer spectroscopy, in *Physical Methods in Bioinorganic Chemistry* (Que, L., Jr., Ed.) pp 287−319, University Science Books, Sausalito, CA.

(20) Omote, Y., Hirama, T., and Komatsu, T. (1974) Dopaquinone and related compounds. Reactions with o-phenylenediamine. *Bull. Chem. Soc. Jpn. 47*, 1957−1959.

(21) Kessel, S. L., Emberson, R. M., Debrunner, P. G., and Hendrickson, D. N. (1980) Iron(III), manganese(III), and cobalt(III) complexes with single chelating o-semiquinone ligands. *Inorg. Chem. 19*, 1170−1178.

(22) Zimmermann, R., Huynh, B. H., Münck, E., and Lipscomb, J. D. (1978) High field Mössbauer studies of reduced protocatechuate 3,4 dioxygenase. *J. Chem. Phys. 69*, 5463−5467.

(23) Neidig, M. L., Kavana, M., Moran, G. R., and Solomon, E. I. (2004) CD and MCD studies of the non-heme ferrous active site in (4-hydroxyphenyl)pyruvate dioxygenase: Correlation between oxygen activation in the extradiol and alpha -KG-dependent dioxygenases. *J. Am. Chem. Soc. 126*, 4486−4487.

(24) Zimmermann, R., and Spiering, H. (1975) Properties of a 5T2 in iron (II) under the action of arbitrary-symmetry ligand fields and spin-orbit coupling I. On the quadrupole splitting. *Phys. Status Solidi 67*, 487−494.

(25) Groce, S. L., and Lipscomb, J. D. (2003) Conversion of extradiol aromatic ring-cleaving homoprotocatechuate 2,3-dioxygenase into an intradiol cleaving enzyme. *J. Am. Chem. Soc. 125*, 11780−11781.

(26) Frazee, R. W., Orville, A. M., Dolbeare, K. B., Yu, H., Ohlendorf, D. H., and Lipscomb, J. D. (1998) The axial tyrosinate Fe^{3+} ligand in protocatechuate 3,4-dioxygenase influences substrate binding and product release: evidence for new reaction cycle intermediates. *Biochemistry 37*, 2131−2144.

(27) Valley, M. P., Brown, C. K., Burk, D. L., Vetting, M. W., Ohlendorf, D. H., and Lipscomb, J. D. (2005) Roles of the equatorial tyrosyl iron ligand of protocatechuate 3,4-dioxygenase in catalysis. *Biochemistry 44*, 11024−11039.

(28) Arciero, D. M., Orville, A. M., and Lipscomb, J. D. (1985) [^{17}O]Water and nitric oxide binding by protocatechuate 4,5-dioxygenase and catechol 2,3-dioxygenase. Evidence for binding of exogenous ligands to the active site Fe^{2+} of extradiol dioxygenases. *J. Biol. Chem. 260*, 14035−14044.

(29) Mabrouk, P. A., Orville, A. M., Lipscomb, J. D., and Solomon, E. I. (1991) Variable-temperature variable-field magnetic circular dichroism studies of the iron(II) active site in metapyrocatechase: implications for the molecular mechanism of extradiol dioxygenases. *J. Am. Chem. Soc. 113*, 4053−4061.

(30) Zhou, J., Kelly, W. L., Bachmann, B. O., Gunsior, M., Townsend, C. A., and Solomon, E. I. (2001) Spectroscopic studies of substrate interactions with clavaminate synthase 2, a multifunctional α-KG-dependent non-heme iron enzyme: Correlation with mechanisms and reactivities. *J. Am. Chem. Soc. 123*, 7388−7398.

(31) Solomon, E. I. (2001) Geometric and electronic structure contributions to function in bioinorganic chemistry: Active sites in non-heme iron enzymes. *Inorg. Chem. 40*, 3656−3669.

(32) Sugimoto, K., Senda, T., Aoshima, H., Masai, E., Fukuda, M., and Mitsui, Y. (1999) Crystal structure of an aromatic ring opening dioxygenase LigAB, a protocatechuate 4,5-dioxygenase, under aerobic conditions. *Structure (London) 7*, 953−965.

(33) Mendel, S., Arndt, A., and Bugg, T. D. H. (2004) Acid-base catalysis in the extradiol catechol dioxygenase reaction mechanism: Site-directed mutagenesis of His-115 and His-179 in *Escherichia coli* 2,3-dihydroxyphenylpropionate 1,2-dioxygenase (MhpB). *Biochemistry 43*, 13390−13396.